Enhanced Photocatalytic Activity of Bismuth-Tungsten Mixed Oxides for Oxidative Decomposition of Acetaldehyde under Visible Light Irradiation

Fumiaki Amano,*[a,b] Kohei Nogami,[b] and Bunsho Ohtani[a,b]

[a]Catalysis Research Center, Hokkaido University, Sapporo 001-0021, Japan.

[b]Graduate School of Environmental Science, Hokkaido University, Sapporo 060-0810, Japan.

*Corresponding author: Fumiaki Amano

Present address: Department of Chemical and Environmental Engineering, The University of Kitakyushu, Kitakyushu 808-0135, Japan.

Tel: +81-93-695-3372,

E-mail: amano@kitakyu-u.ac.jp

Abstract Russelite bismuth tungstate (Bi_2WO_6) flake-ball particles prepared by a hydrothermal reaction method have been reported to be visible-light-responsive photocatalysts for mineralization of organic compounds. Here, we report new bismuth-tungsten mixed oxide particles with a tungsten-to-bismuth ratio (W/Bi ratio) in feed of 1.0, which is two-times higher than the stoichiometric ratio of Bi_2WO_6 (W/Bi = 0.50). Compared to the conventional Bi_2WO_6 flake-ball particles, the tungsten-rich particles exhibited a narrow band gap (2.70 eV), large specific surface area due to the rectangular platelet nanostructure, and high level of photocatalytic activity for oxidative decomposition of acetaldehyde.

Keywords Photocatalysis; Bi_2WO_6; Aurivillius phase; Nanoplate; Visible light

1. Introduction

Titania is one of the most famous semiconductor photocatalysts. Photoabsorption generates a

pair of a photoexcited electron and positive hole, which reacts with species adsorbed on the surface to induce reduction and oxidation competing with the recombination of a pair. Anatase titania is known to induce photocatalytic oxidative decomposition of organic compounds into carbon dioxide (CO_2) and water, i.e. mineralization. However, it works only under ultraviolet (UV) light irradiation due to the wide band gap of 3.2 eV. Actually, a pristine titania photocatalyst is less active for purification of indoor air, since the intensity of UV light emitted from a fluorescent light tube is very low. In this sense, development of visible-light-responsive photocatalysts with high levels of activity is still one of the research fields of photocatalyst materials [1-7].

Recently, much attention has been focused on russelite bismuth tungstate (Bi_2WO_6) and composite materials as visible-light-responsive photocatalysts [8-13]. Bi_2WO_6 is the n = 1 member of the family $(Bi_2O_2)(B^{4+}_{n}O_{3n+1})$ of cation-deficient bismuth-layered compounds (Aurivillius phase, B = Mo, W, *etc.*) [14]. We have reported that Bi_2WO_6 flake-ball particles, which are micrometer-sized spherical assemblies of polycrystalline flakes comprised of rectangular single-crystalline platelets, exhibited a high level of photocatalytic activity for mineralization of acetaldehyde and acetic acid [15,16]. The onset wavelength of action spectrum for the reaction was located at 440 nm, and this wavelength corresponds to the band gap energy of ca. 2.8 eV [17,18]. The apparent quantum efficiency at 400 nm was measured to be 3–8%, depending on the kind of reaction [17,18]. Unfortunately, visible-light absorption is not sufficient and quantum efficiency should still be improved. Flake-ball particles prepared under the condition of an atomic ratio of tungsten to bismuth (W/Bi ratio) of 0.55 exhibited a photocatalytic activity level higher than that of particles prepared at a stoichiometric W/Bi ratio, i.e., 0.50 [16]. This result suggests that the W/Bi ratio might significantly affect physicochemical properties of Bi_2WO_6 particles. In the present study, we found that tungsten-rich bismuth tungsten mixed oxide particles with a high W/Bi ratio (1.0) exhibited a level of photocatalytic activity higher than that of conventional Bi_2WO_6 flake-ball particles (W/Bi ratio = 0.55). Unexpectedly, the crystal composition of the newly developed particles was similar to that of Bi_2WO_6 rather than double-layered cation-deficient

Aurivillius-phase bismuth tungstate ($Bi_2W_2O_9$), the W/Bi ratio of which is 1.0. $Bi_2W_2O_9$ is the n = 2 member of the $(Bi_2O_2)(B^{4+}_nO_{3n+1})$ family and has been reported as a photocatalyst with a band gap of 2.95 eV [8,19]. Based on the specific surface area and photoabsorption ability, the enhanced photocatalytic activities of the newly developed tungsten-rich particles are discussed.

2. Experimental

2.1. Preparation

Bismuth tungstate particles were prepared by hydrothermal reaction of a mixture of bismuth nitrate (5.0 mmol) and an aqueous solution of sodium tungstate (2.75 and 5.0 mmol for W/Bi ratios of 0.55 and 1.0, respectively). The mixture suspended in an aqueous solution of ca. 80 mL was heated in a 100-mL Teflon-lined autoclave at 160 °C for 20 h. The solution was strongly acidic due to hydrolysis of bismuth nitrate. After the hydrothermal reaction under auto-generated pressure and cooling to room temperature, the precipitates were washed with Milli-Q water three times and dried at 393 K in air.

2.2 Characterization

Scanning electron microscope (SEM) images were observed by a JEOL JSM-7400F field emission SEM. The chemical compositions were analyzed by a JEOL JED-2300 energy dispersive X-ray spectrometer (EDS) and JEOL JPS-9010MC X-ray photoelectron spectrometer (XPS) with Mg Kα radiation. Specific surface area of the samples was analyzed by the Brunauer–Emmett–Teller (BET) method from nitrogen adsorption isotherms at -196 °C. X-ray diffraction (XRD) patterns were recorded on a Rigaku RINT ULTIMA diffractometer with Cu Kα radiation. UV-visible diffuse reflection spectra were recorded using barium sulfate as a standard material by a JASCO V-670 spectrometer with a JASCO PIN-757 integrating sphere. Transmission electron microscope (TEM) images and selected area electron diffraction (SAED) patterns were recorded on a JEOL JEM-2100F field emission TEM.

2.3. Photocatalytic activity test

Photocatalyst powder (50 mg) spread on a glass plate (15 mm × 15 mm) was placed on the bottom of a cylindrical glass vessel (ca. 330 mL) filled with ambient air. After adsorption of gaseous acetaldehyde (1100 ppm, ca. 15 μmol) had reached equilibrium in the dark, photoirradiation was performed using a 300-W xenon arc lamp (ILC Technology CERMAX-LX300F) with a cold filter at room temperature. Irradiance from the lamp is shown in Fig. S1 in Supplementary data. The amounts of CO_2 and acetaldehyde were measured by a TCD micro-gas chromatograph (Agilent Technologies 3000A Micro GC). An L-42 cut-off filter and a Y-44 cut-off filter (Asahi Techno Glass) were used for irradiation at wavelengths longer than 400 nm and 420 nm, respectively. The cut-off positions specified at 50% internal transmittance were ca. 420 and 440 nm for L-42 and Y-44 cut-off filters, respectively.

3. Results and Discussion

3.1. Morphology of particles

As previously reported, the particles prepared at W/Bi = 0.55 exhibited a flake-ball structure with averaged diameter of ca. 5 μm [15,16]. The flakes were comprised of rectangular platelets with average thickness of ca. 30 nm. Figure 1 shows SEM images of the bismuth-tungsten mixed oxide particles prepared in a tungsten-rich condition (W/Bi = 1.0). Micrometer-scaled spherical particles were observed as in the case of flake-ball particles, but the average diameter (ca. 15 μm) was larger than that of flake-ball particles. A number of rectangular platelets with thickness of ca. 20 nm had densely accumulated to form spherical particles. The uniform platelet nanostructure suggested that the crystalline composition would be homogeneous. The particles prepared at W/Bi = 1.0 exhibited a BET specific surface area of 47.5 $m^2 g^{-1}$, which was larger than that of flake-ball particles (W/Bi = 0.55, 19.3 $m^2 g^{-1}$). The increment of surface area might be due to the decrease in thickness of rectangular platelets. Nanometer-sized void spaces were present between the platelets comprising of micrometer-scaled spherical particles. Such nanostructures are effective for forming materials with a large surface area to volume ratio.

3.2. Crystal composition

The W/Bi ratios estimated by EDS were 0.58 ± 0.05 for flake-ball particles (W/Bi = 0.55) and 0.98 ± 0.10 for particles prepared at W/Bi = 1.0. The chemical composition in feed for preparation was found to be maintained in each powder sample. Figure 2 shows XRD patterns of the hydrothermally-prepared bismuth-tungsten mixed oxide particles. Flake-ball particles (W/Bi = 0.55) exhibited a crystal structure of Bi_2WO_6 comprised of Bi_2O_2 sheets interleaved with corner-sharing WO_6 octahedral sheets [14]. The XRD pattern of the newly prepared tungsten-rich particles (W/Bi =1.0) was similar to that of Bi_2WO_6 (PDF #39-0256), although the peaks were broad and weak. It should be noted that there is a diffraction peak at $2\theta = 23.3°$ that is difficult to assign to a crystal phase. Cation-deficient Aurivillius-phase $Bi_2W_2O_9$, which is comprised of Bi_2O_2 sheets interleaved with double-layered W_2O_7 octahedral sheets [14], exhibited a W/Bi ratio of 1.0. However, the tungsten-rich particles (W/Bi = 1.0) exhibited a crystal structure similar to that of single-layered Bi_2WO_6 rather than double-layered $Bi_2W_2O_9$ (PDF #33-0221, Fig. S2 in Supplementary data shows XRD pattern of $Bi_2W_2O_9$ powders). The W/Bi ratios estimated by XPS were 0.52 and 0.84 for flake-ball particles (W/Bi = 0.55) and tungsten-rich particles (W/Bi = 1.0), respectively. The detection depth of XPS is shallow, and therefore the result corresponds to the composition of the outermost surface of the particles. The ratios estimated by XPS were consistent with the ratios estimated by EDS in an acceptable error range, suggesting that an excess amount of tungsten to the stoichiometric ratio was included in the sample uniformly and not segregated on the outermost surface as amorphous tungsten oxides.

3.3 Photoabsorption

Figure 3 shows UV-visible diffuse reflection spectra of the bismuth-tungsten mixed oxide particles and commercial titania P25 (Nippon Aerosil). The photoabsorption edge of tungsten-rich particles (W/Bi = 1.0) was located at ca. 470 nm, which is a wavelength longer than the edge of flake-ball particles (W/Bi = 0.55). This suggests that excess amount of tungsten resulted in enhanced photoabsorption of the violet portion of the visible light spectrum. The absence of crystalline tungsten trioxide (WO_3) with a band gap of ca. 2.7 eV was confirmed by XRD

measurement, and there was no segregation of amorphous WO_3 on the surface as indicated by XPS analysis. If the sample is not pure phase, but consists of Bi_2WO_6 and another compound such as tungsten oxides, there should be a shoulder in the photoabsorption edge. The steep rise in photoabsorption suggests that the sample is homogeneous. The band gap estimated using Tauc plot assuming indirect allowed transition (plot of $[F(R)\ h\nu]^{0.5}$ against $h\nu$, where $F(R)$ is Kubelka-Munk function and $h\nu$ is incident photon energy) was 2.70 eV for the particles (W/Bi = 1.0). Quantum size effect predicts that the optical band gap should be widened when the crystalline size decreases. It has been reported that Bi_2WO_6 macroparticles prepared by the conventional solid state reaction exhibited a band gap of ca. 2.6 eV [16]. Although the crystalline size of tungsten-rich particles was smaller than that of Bi_2WO_6 flake-ball particles, the band gap was narrower than that of flake-ball particles, which was 2.82 eV. The difference in the band gaps (electronic band structures) might be related to the difference in crystal structure, since the crystal composition of tungsten-rich particles is suggested to be different from that of Bi_2WO_6. The band gap energies of the prepared particles were smaller than that of titania P25, which is a mixture of anatase (band gap of 3.2 eV) and rutile (band gap of 3.0 eV). It should be noted that the active phase for photocatalytic oxidative decomposition of acetaldehyde was revealed to be anatase by means of action spectrum analysis [20,21].

3.4 Crystalline orientation

Figure 4 shows TEM images and SAED patterns of platelets derived from Bi_2WO_6 flake-ball particles (W/Bi = 0.55) and tungsten-rich particles. The ordered spots within the SAED patterns indicate that both platelets possess single crystalline nature. For platelet derived from flake-ball particles, the lattice spacing of 0.273, 0.272, and 0.193 nm was consistent with the interplanar distances of {200}, {002}, and {202} of Bi_2WO_6 (PDF #39-0256), respectively. The direction of [-202] and [202] were parallel to the side edges of the platelet. These results indicate that Bi_2WO_6 platelets exhibit a large rectangular surface of the {010} facet and sides of {-101} and {101} facets. The SAED pattern of platelets derived from tungsten-rich particles was very similar to that of

Bi_2WO_6 platelets, suggesting that the crystal lattice planes along the [010] zone axis was similar to that of Bi_2WO_6. However, the crystal structure should be different from that of Bi_2WO_6, since the crystal composition was different from that of Bi_2WO_6. There might be difference in the lattice constant along the *b* axis. The SAED analysis suggested that the tungsten-rich particles were composed of single-crystalline platelets of bismuth tungstate.***3.5 Photocatalytic activity***

Photoexcited electrons and holes of Bi_2WO_6 photocatalysts can induce reduction of molecular oxygen into water and oxidation of organic compounds into CO_2, respectively. Figure 5 shows time courses of CO_2 liberation through photocatalytic oxidative decomposition of gaseous acetaldehyde (ca. 15 μmol) in air. The overall reaction could be expressed as follows: $CH_3CHO + 5/2O_2 \rightarrow 2CO_2 + 2H_2O$. Decrease in the amount of gas-phase acetaldehyde to be below the detectable limit and molar amount of CO_2 liberation (ca. 30 μmol) two-times larger than that of acetaldehyde in feed were confirmed over each photocatalyst under full arc irradiation. No organic intermediate was detected in the gas phase. For the conditions under full arc irradiation including UV light, the rate of CO_2 liberation was increased in the order of flake-ball particles (W/Bi = 0.55) < tungsten-rich particles (W/Bi = 1.0) < titania P25. The BET specific surface area of P25 was ca. 48 $m^2 g^{-1}$, similar to that of tungsten-rich particles (W/Bi = 1.0). As expected from the band gap of anatase, P25 exhibited negligible liberation of CO_2 under irradiation at wavelength >400 nm. On the other hand, the bismuth-tungstate mixed oxide particles showed visible-light response for mineralization of acetaldehyde. Tungsten-rich particles (W/Bi = 1.0) exhibited a higher CO_2 liberation rate than that of flake-ball particles (W/Bi = 0.55). We have reported that rate of acetaldehyde degradation was expressed by first-order kinetics with respect to the amount of surface-adsorbed acetaldehyde when Bi_2WO_6 flake-ball particles exhibited similar levels of crystalline content, and the capacity for reactant adsorption was proportional to the specific surface area [22]. A subsequent study revealed that efficiency for the photocatalytic reaction showed a proportional relation with specific surface area rather than crystalline content of Bi_2WO_6 flake-ball particles [23]. Therefore, the enhancement of CO_2 liberation rate could be

assignable to increase in the specific surface area by increasing the amount of tungsten from W/Bi = 0.55 to 1.0. This positive effect can overcome the negative effect due to the decrease in crystallinity, which might enhance electron-hole recombination [23]. When the optical filter was changed from L-42 to Y-44, the CO_2 liberation after 20-min photoirradiation was reduced from 6.0 μmol to 3.1 μmol for tungsten-rich particles (W/Bi = 1.0) and was reduced from 2.6 μmol to 0.3 μmol for flake-ball particles (W/Bi = 0.55). This indicates that tungsten-rich particles (W/Bi = 1.0) still exhibited considerable photocatalytic activity under irradiation at wavelength >420 nm, since the photoabsorption edge was red-shifted in comparison with the edge of flake-ball particles. It was confirmed that the narrow band gap enhanced the photocatalytic activity under visible light irradiation. After prolonged irradiation (ca. 15 h), almost complete oxidative decomposition of acetaldehyde into CO_2 was confirmed even under visible light irradiation at wavelength >420 nm (Fig. S3 in Supplementary data). It was possible to use the photocatalysts for reactions several times without deactivation and for mineralization of other organic compounds such as acetic acid, which might be an intermediate in photocatalytic oxidation of acetaldehyde. Although the crystal structure is unknown, it is concluded that the tungsten-rich bismuth-tungstate mixed oxides are visible-light-responsive photocatalysts for mineralization of organic compounds.

4. Conclusion

New bismuth-tungsten mixed oxide particles were prepared by a hydrothermal preparation method using starting materials with a W/Bi ratio of 1.0. The tungsten-rich particles included tungsten and bismuth with that ratio in feed, but the crystal structure was ambiguous; unexpectedly, the XRD and SAED patterns were similar to that of single-layered Bi_2WO_6 rather than those of double-layered $Bi_2W_2O_9$. It should be noted that the tungsten-rich rectangular platelets were single crystal, suggesting that the crystal structure would be new. The particles with new crystal composition exhibited a high level of visible-light-responsive activity for oxidative decomposition of gaseous acetaldehyde, probably due to the large surface area (47.5 m^2 g^{-1}) and the narrow band gap (2.70 eV) compared to those of conventional Bi_2WO_6 flake-ball particles (specific surface area

of 19.3 m^2 g^{-1} and band gap of 2.82 eV). It should be noted that the long lifetime of photoexcited carriers in the new crystalline compound would also be the one of the reasons for the enhanced photocatalytic activity.

Acknowledgement

This work was supported by a Grant-in-Aid for Young Scientists (B) (No. 21750202) from the Ministry of Education, Culture, Sports, Science and Technology (MEXT), Japan.

References

[1] N. Murakami, T. Matsuo, T. Tsubota, T. Ohno, Catal. Commun. 12 (2011) 341-344.

[2] X.Q. Qiu, M. Miyauchi, H.G. Yu, H. Irie, K. Hashimoto, J. Am. Chem. Soc. 132 (2010) 15259-15267.

[3] N. Murakami, A. Ono, M. Nakamura, T. Tsubota, T. Ohno, Appl. Catal., B 97 (2010) 115-119.

[4] H. Kominami, A. Tanaka, K. Hashimoto, Chem. Commun. 46 (2010) 1287-1289.

[5] S. Kitano, K. Hashimoto, H. Kominami, Chem. Lett. 39 (2010) 627-629.

[6] Z.F. Liu, Z.G. Zhao, M. Miyauchi, J. Phys. Chem. C 113 (2009) 17132-17137.

[7] H.G. Kim, P.H. Borse, J.S. Jang, E.D. Jeong, O.S. Jung, Y.J. Suh, J.S. Lee, Chem. Commun. (2009) 5889-5891.

[8] A. Kudo, S. Hijii, Chem. Lett. 28 (1999) 1103-1104.

[9] J.W. Tang, Z.G. Zou, J.H. Ye, Catal. Lett. 92 (2004) 53-56.

[10] H.B. Fu, C.S. Pan, W.Q. Yao, Y.F. Zhu, J. Phys. Chem. B 109 (2005) 22432-22439.

[11] L.H. Zhang, W.Z. Wang, Z.G. Chen, L. Zhou, H.L. Xu, W. Zhu, J. Mater. Chem. 17 (2007) 2526-2532.

[12] L.W. Zhang, Y.J. Wang, H.Y. Cheng, W.Q. Yao, Y.F. Zhu, Adv. Mater. 21 (2009) 1286-1290.

[13] Q. Xiao, J. Zhang, C. Xiao, X.K. Tan, Catal. Commun. 9 (2008) 1247-1253.

[14] J.C. Champarnaud-Mesjard, B. Frit, A. Watanabe, J. Mater. Chem. 9 (1999) 1319-1322.

[15] F. Amano, K. Nogami, R. Abe, B. Ohtani, Chem. Lett. 36 (2007) 1314-1315.

[16] F. Amano, K. Nogami, R. Abe, B. Ohtani, J. Phys. Chem. C 112 (2008) 9320-9326.

[17] F. Amano, K. Nogami, B. Ohtani, J. Phys. Chem. C 113 (2009) 1536-1542.

[18] F. Amano, A. Yamakata, K. Nogami, M. Osawa, B. Ohtani, J. Am. Chem. Soc. 130 (2008) 17650-17651.

[19] J.W. Tang, J.H. Ye, J. Mater. Chem. 15 (2005) 4246-4251.

[20] T. Torimoto, N. Nakamura, S. Ikeda, B. Ohtani, Phys. Chem. Chem. Phys. 4 (2002) 5910-5914.

[21] F. Amano, M. Tanaka, B. Ohtani, Catal. Lett. 140 (2010) 27-31.

[22] F. Amano, K. Nogami, M. Tanaka, B. Ohtani, Langmuir 26 (2010) 7174-7180.

[23] F. Amano, A. Yamakata, K. Nogami, M. Osawa, B. Ohtani, J. Phys. Chem. C 115 (2011) 16598-16605.

Figure Captions

Figure 1. SEM images of bismuth-tungsten mixed oxide particles prepared at W/Bi = 1.0.

Figure 2. XRD patterns of the newly prepared tungsten-rich particles (W/Bi = 1.0) and Bi_2WO_6 flake-ball particles (W/Bi = 0.55). Bragg reflections due to Bi_2WO_6 are indicated by the indices.

Figure 3. UV-visible diffuse reflection spectra of (a) tungsten-rich particles (W/Bi = 1.0), (b) flake-ball particles (W/Bi = 0.55), and (c) commercial titania P25. Inset shows Tauc plot of tungsten-rich particles.

Figure 4. TEM images and SAED patterns of rectangular platelets derived from (a) flake-ball particles (W/Bi = 0.55) and (b) tungsten-rich particles (W/Bi = 1.0).

Figure 5. Time courses of photocatalytic CO_2 liberation from oxidative decomposition of acetaldehyde over (a) tungsten-rich particles (W/Bi = 1.0), (b) flake-ball particles (W/Bi = 0.55), and (c) commercial titania P25: (A) full-arc irradiation, (B) irradiation with an L-42 filter (wavelength >400 nm), and (C) irradiation with a Y-44 filter (wavelength >420 nm).

Figure 1

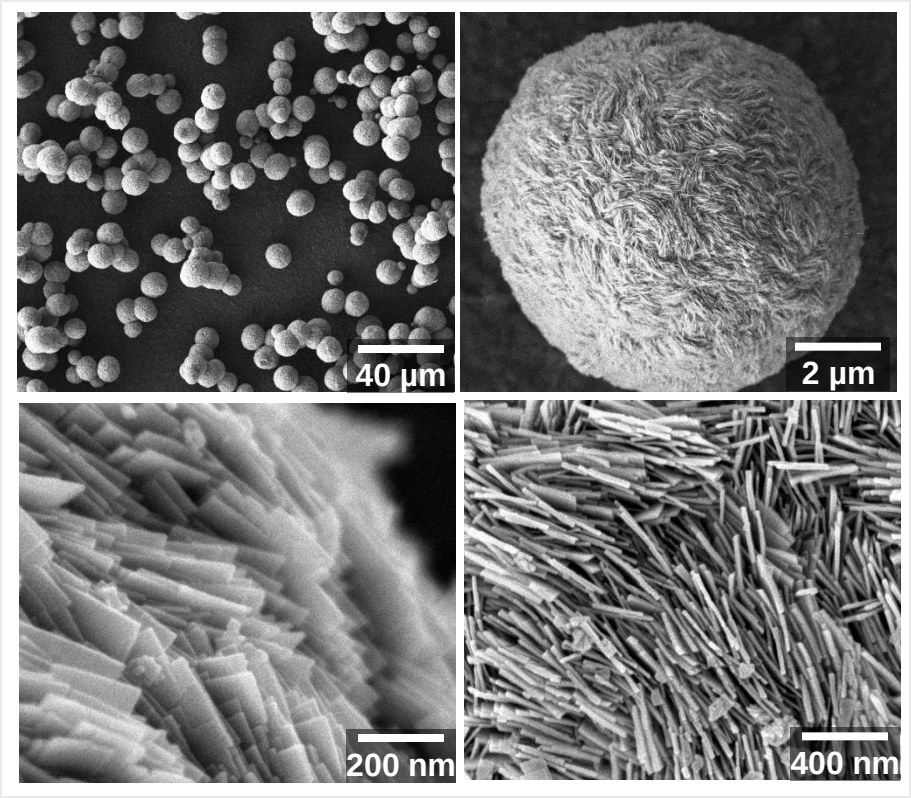

Figure 2

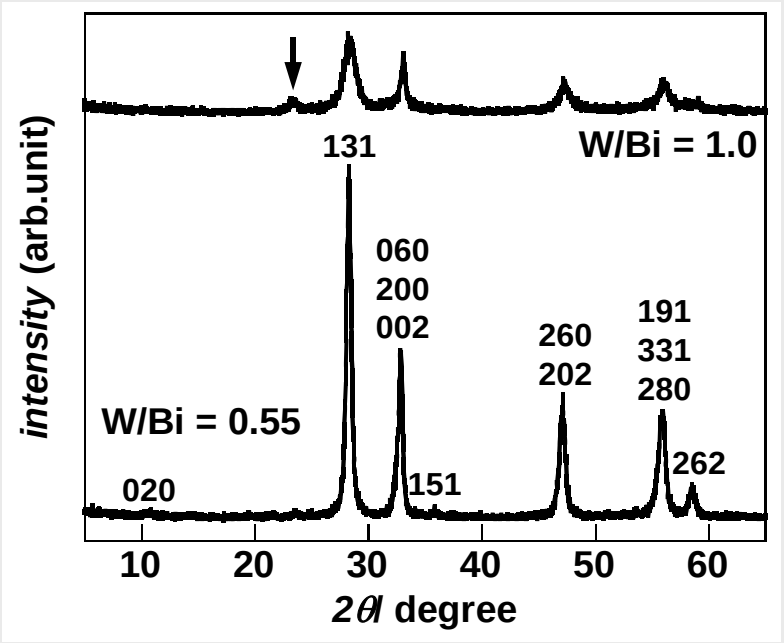
intensity (arb.unit)
131
W/Bi = 1.0
060
200
002
260
202
191
331
280
W/Bi = 0.55
020
151
262
10
20
30
40
50
60
2θ/ degree

Figure 3

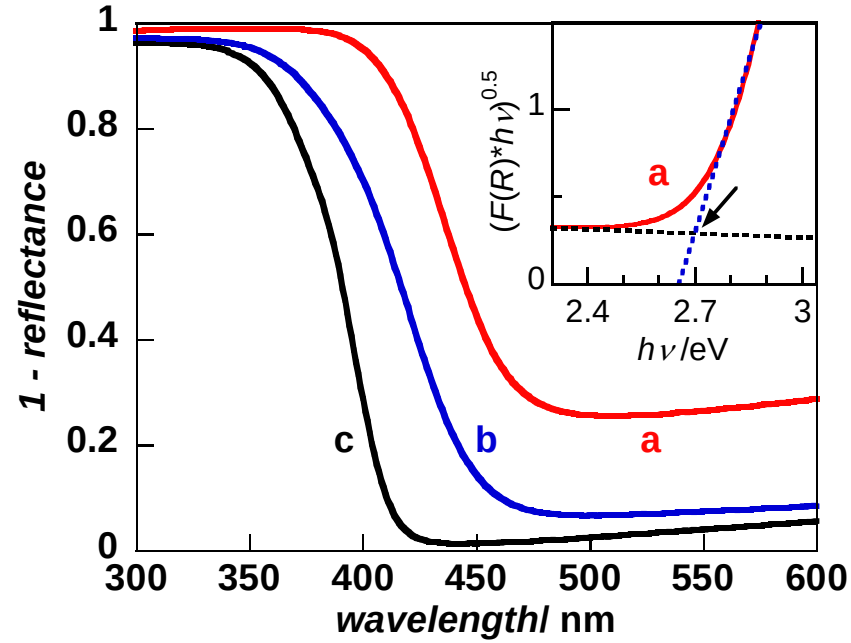
1
0.8
0.6
0.4
0.2
0
1 - reflectance
300
350
400
450
500
550
600
wavelength/ nm
c
b
a
(F(R)*hν)^0.5
1
0
a
2.4
2.7
3
hν/eV

Figure 4

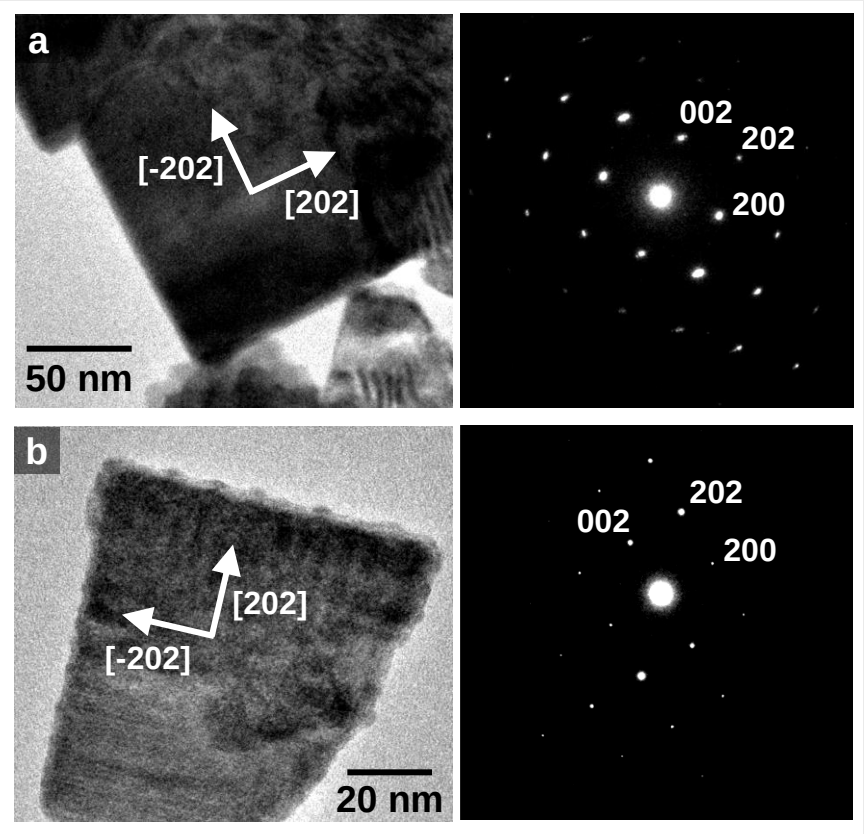

Figure 5

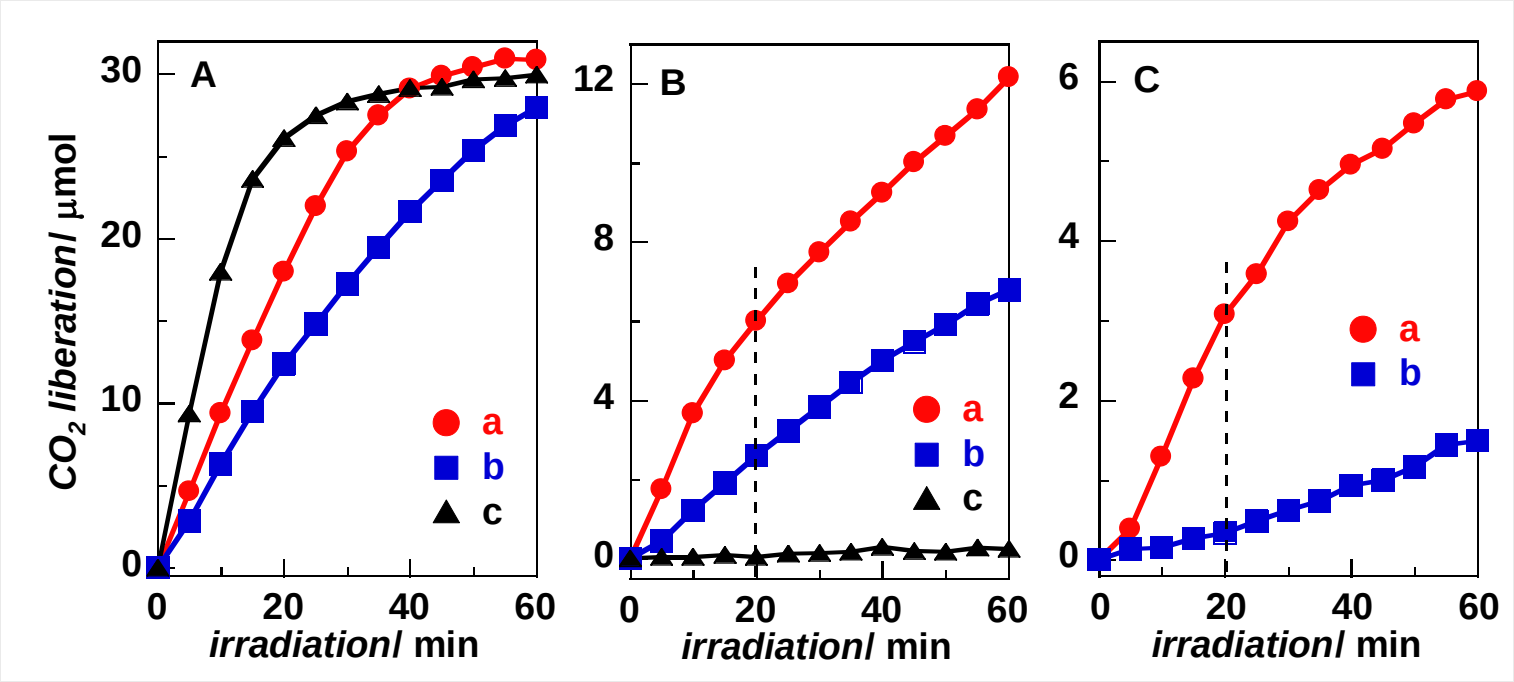
A
B
C
CO_2 liberation/ μmol
irradiation/ min
a
b
c
0
10
20
30
4
8
12
2
6
0
20
40
60

Figure 3 (black and white)

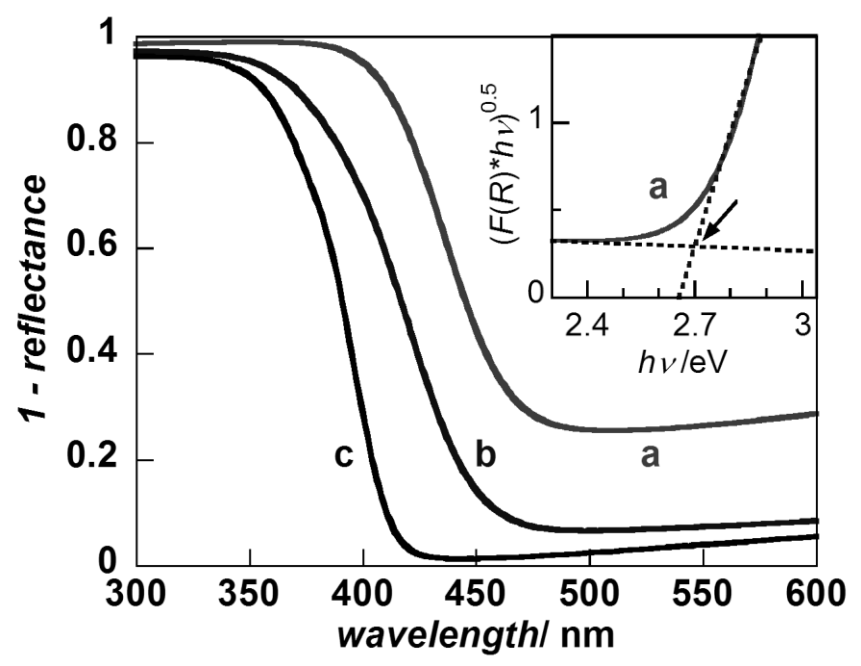

Figure 5 (black and white)